Flexible Optical Waveguide Film Fabrications and Optoelectronic Devices Integration for Fully Embedded Board-Level Optical Interconnects

Chulchae Choi, Lei Lin, *Member, IEEE*, Yujie Liu, Jinho Choi, Li Wang, David Haas, Jerry Magera, and Ray T. Chen, *Fellow, IEEE, Fellow, OSA*

***Abstract*—This paper demonstrates a flexible optical waveguide film with integrated optoelectronic devices (vertical-cavity surface-emitting laser (VCSEL) and p-i-n photodiode arrays) for fully embedded board-level optical interconnects. The optical waveguide circuit with 45° micromirror couplers was fabricated on a thin flexible polymeric substrate by soft molding. The 45° couplers were fabricated by cutting the waveguide with a microtome blade. The waveguide core material was SU-8 photoresist, and the cladding was cycloolefin copolymer. A thin VCSEL and p-i-n photodiode array were directly integrated on the waveguide film. Measured propagation loss of a waveguide was 0.6 dB/cm at 850 nm.**

***Index Terms*—embedded optical interconnects, 45° micromirror coupler, printed circuit board (PCB), poly(dimethylsiloxane) (PDMS), soft molding, SU-8, topas, vertical-cavity surface-emitting laser (VCSEL), waveguide film.**

I. Introduction

THE speed and complexity of integrated circuits are increasing rapidly as integrated circuit technology advances from very-large-scale integrated (VLSI) circuits to ultra-large-scale integrated (ULSI) circuits. As the number of devices per chip, the number of chips per board, the modulation speed, and the degree of integration continue to increase, electrical interconnects are facing their fundamental bottlenecks, such as speed, packaging, fan-out, and power dissipation. In the quest for high-density packaging of electronic circuits, the construction of multichip modules (MCM), which decrease the surface area by removing package walls between chips, improved signal integrity by shortening interconnection distances and removing impedance problems and capacitances [1], [2].

The employment of copper and materials with lower dielectric constant materials can release the bottleneck in a chip level for the next several years. The International Technology Roadmap for Semiconductors (ITRS) expects that on-chip local clock speed will constantly increase to 10 GHz by the year 2011. On the other hand, chip-to-board clock speed is expected to have a slow increasing rate after the year 2002 [3]. The interconnection speed of a copper line on a printed circuit board cannot run over a few gigahertz [4]. High-performance materials and advanced layout technology such as IMPS (Interconnected Mesh Power system) are introduced [5]. In particular, IMPS is focused on the signal integrity, such as controlled impedance signal transmission with very low crosstalk. The electrical interconnection described by Walker *et al.* provides a 10-Gb/s link over a distance of less than 20 m using coaxial cable [6]. However, coaxial cabling is bulky; therefore, it is not suitable for a high-density interconnection application. Electrical interconnects operating at a high-frequency region have many problems to be solved, such as crosstalk, impedance matching, power dissipation, skew, and packing density. There is a little hope for solving all of the problems. However, optical interconnection has several advantages, such as immunity to the electromagnetic interference, independency to impedance mismatch, less power consumption, and high-speed operation. Although the optical interconnects have great advantages compared with the copper interconnection, they still have some difficulties regarding packaging, multilayer technology, signal tapping, and reworkability.

Several optical interconnect techniques such as free space, guided wave, board level, and fiber array interconnections were introduced for system-level applications [7]–[11]. They successfully demonstrated high-speed optical interconnection; however, there were still packaging difficulties.

This paper introduces fully embedded board-level optical interconnects to relieve packaging difficulty. This paper presents a flexible optical waveguide, thermal management of embedded thin-film vertical-cavity surface-emitting lasers (VCSELs), and an optical interconnection layer integrated with thin-film VCSELs and photodetector arrays.

II. Fully Embedded Board-Level Optical Interconnects

A fully embedded board-level guided-wave optical interconnection is presented in Fig. 1, where all elements involved in providing high-speed optical communications within a board are shown. These include a VCSEL, surface-normal waveguide couplers, and a polymer-based channel waveguide functioning as the physical layer of optical interconnection. The driving electrical signals to modulate the VCSEL and the demodulated signals received at the photoreceiver flow through electrical vias connecting to the surface of the PC board. The fully embedded structure makes the insertion of optoelectronic components into microelectronic systems much more realistic when considering the fact that the major stumbling block for implementing optical interconnection onto high-performance microelectronics is

Manuscript received January 5, 2004.

C. Choi, L. Lin, Y. Liu, J. Choi, and R. T. Chen are with the University of Texas at Austin, Austin, TX 78712-1157 USA.

D. Haas and J. Magera are with SANMINA-SCI, Owego, NY 13827 USA.

Digital Object Identifier 10.1109/JLT.2004.833815

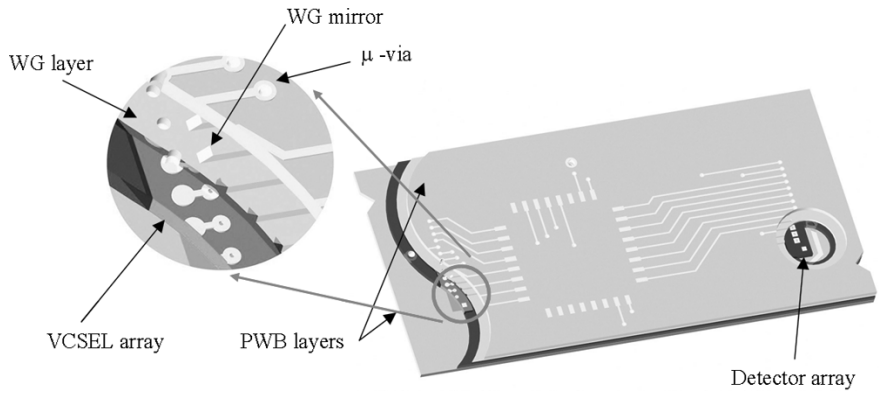

Fig. 1. Illustration of fully embedded board-level optical interconnects.

the packaging incompatibility. All the real estate of the printed circuit board (PCB) surface is occupied by electronics not by optoelectronic components. The performance enhancement due to the employment of the optical interconnection is observed. Unlike conventional approaches, there is no interface problem between electronic and optoelectronic components.

To realize fully embedded board-level optical interconnects, many stumbling blocks are to be solved, such as a thin-film transmitter and detector, thermal management, process compatibility, reliability, a cost-effective fabrication process, and easy integration.

The research work presented herein eventually will relieve such concerns and make the integration of optical interconnection highly feasible.

III. 45° Waveguide Mirror Coupler

To efficiently couple optical signals from VCSELs to polymer waveguides and then from waveguides to photodetectors, two types of waveguide couplers are investigated: tilted grating couplers and 45° waveguide mirrors. There are a large number of publications in grating design [12]–[16]. However, the surface-normal coupling scenario in optical waveguides has not been carefully investigated so far. The profile of tilted grating greatly enhances the coupling efficiency in the desired direction. A very important aspect of manufacturing of such couplers is the tolerance interval of the profile parameters, such as the tooth height, the width, and the tilt angle. However, the tilted grating coupler has inherent wavelength sensitivity and is not applicable for planarized waveguide.

The 45° waveguide mirror coupler is a very critical component in optical interconnection applications especially in planarized lightwave circuits (PLCs). The mirror can be incorporated with a vertical optical via to enable three-dimensional optical interconnects and couples light to the waveguide. The 45° waveguide mirror is insensitive to the wavelength of light and has high coupling efficiency. There are various techniques to fabricate a 45° mirror such as laser ablation [17], oblique reactive ion etching (RIE) [18], temperature-controlled RIE [19], reflow [20], and machining [21]. The laser ablation method is subjected to lower throughput and surface damage. The oblique RIE method is limited by directional freedom. The temperature-controlled RIE method is free from directional freedom, but the quality of the mirror depends on process and materials.

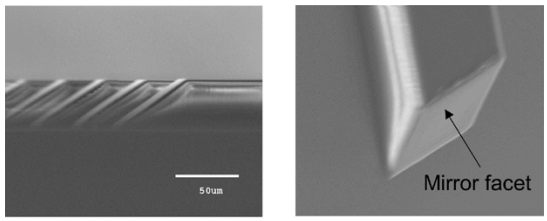

Fig. 2. (a) Scanning electron microscopy (SEM) photograph of the waveguide structures with 45° waveguide mirrors. (b) Enlarged view of the mirror surface.

The reflow method is also subjected to lower throughput. The machining provides good surface profile; however, it is difficult to cut an individual waveguide on a substrate due to the physical size of the machining tool. We developed a new fabrication method using a microtome blade. Polymers can be cut with a very sharp blade. Based on this fact, a simple fabricating technique was developed. A blade sliding down to the waveguide substrate at 45° slope cuts the waveguides at 45°. It is like a guillotine sliding on a slope. The difference is that the blade of the guillotine falls at the right angle; on the other hand, the blade falls at 45°.

The material of the master waveguide structure is SU-8 (by MicroChem) photoresist. The 45° waveguide mirror was fabricated by a mtilted microtome setup. The master waveguide structure was kept at 120 °C on a hot plate. In general, elevated temperature soften polymer. The softness ends up with smoother cutting surface. The blade was sliding down on substrate at 45° slope. The side-off view and surface of the mirror is shown in the Fig. 2. All waveguides were cut simultaneously by the microtome blade.

The coupling efficiency is one of the most critical issues in the fully embedded optical interconnects because of the concerns about thermal management and crosstalk. Higher coupling efficiency between the waveguide and the VCSEL or detector enables the lower power operation of the VCSEL. Furthermore, when a small-aperture VCSEL is used to operate at a high speed, for example, a 3-μm aperture for a 10-GHz operation, the coupling efficiency is of paramount concern because of the large spatial divergence of the VCSEL's light. A large-aperture selectively oxidized VCSEL operates in multiple transverse modes due to the strong index confinement created by an oxide layer with a low refractive index [22]. Various

techniques were introduced to operate in single transverse mode [23]–[25]. Real spatial distribution of the VCSEL is not the same as the Gaussian profile; however, we can consider it as a Gaussian profile by ignoring small discrepancies. This assumption results in a simple calculation. Another assumption is that lights within the acceptance angle of the waveguide are totally coupled into the waveguide. There are approximately ten supporting modes in the 50×50-μm waveguide with $\Delta n = 0.01$. For an exact calculation, we have to consider all the modes, but the number of mode is quite large. It can be treated as geometrical optics. The coupling efficiency η can be calculated by the ratio of coupled power to total laser power, as follows:

$$\eta = \frac{\int_{-r_c}^{r_c} |E(r,z)|^2 \, dr}{\int_0^{\infty} |E(r,0)|^2 \, dr} = \left(\frac{\omega_0}{\omega(z)}\right)^2 \int_{-r_c}^{r_c} |E(r,z)|^2 \, dr$$

where $\boldsymbol{r}_c$ is the maximum radius at the mirror facet which corresponds to the acceptance angle of the waveguide.

The coupling efficiencies between VCSEL and square (50×50-μm) waveguide with $\Delta n = 0.01$ (the refractive-index difference between core and cladding) were calculated as a function of angular deviation from 45°. The substrate thickness (bottom cladding) and the aperture of the VCSEL are 127 and 12 μm, respectively. The coupling efficiencies between VCSEL and square (50×50-mm) waveguide with $\Delta n = 0.01$ (the refractive-index difference between core and cladding) were calculated as a function of angular deviation from 45°. The substrate thickness (bottom cladding) and the aperture of the VCSEL are 127 and 12 mm, respectively.

Fig. 3 shows the intensity distributions of laser light at the mirror surface and the coupling efficiencies as a function of angular deviation from 45° for a 127-μm-thick substrate, a 50×50-μm waveguide, and a VCSEL with 12-μm aperture. The facet of the 45° mirror was coated with aluminum to ensure the reflection because total internal reflection (TIR) does not occur due to the top cladding layer. The reflectance of the aluminum is about 92%. In this scheme, all laser lights fall within the mirror. The coupling efficiency is 92%, which means nearly 100% of the light is coupled into the waveguide, excluding the reflectance due to aluminum. Fig. 5 shows the coupling efficiency as a function of angular deviation from 45°. The coupling efficiency maintains constant values within $45° \pm 1.5°$ mirror angle. Therefore, the mirror angle should be kept within $45° \pm 1.5°$.The coupling efficiency drops dramatically when the mirror angle is out of the tolerance range ($\pm 1.5°$).

IV. Master Fabrication for Mold

There are various fabricating techniques to define an optical waveguide on myriads of substrates. The RIE uses ionized gas to remove material where it is not protected by a mask material in a vacuum chamber. The size of the substrate purely depends on the vacuum chamber. It is relatively free from material selection because RIE is a physical removing process. The lithography uses optically transparent and photosensitive materials. An exposed or unexposed area by ultraviolet (UV) light makes the material insoluble to a solvent due to the cross linking of molecules.

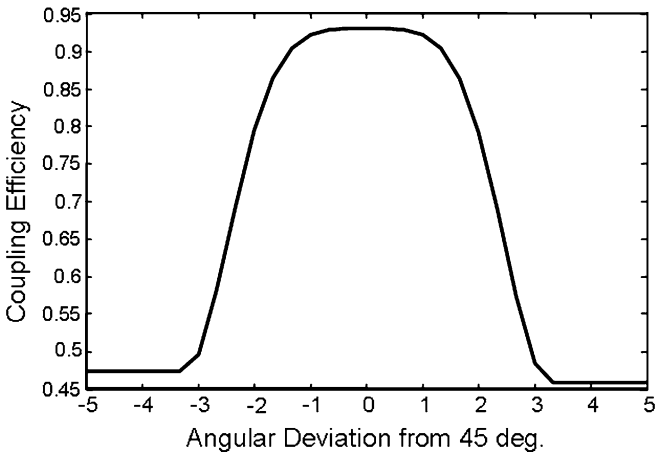

Fig. 3. Coupling efficiencies as a function of angular deviation from 45° for a 127-μm-thick substrate with a 12-μm aperture VCSEL.

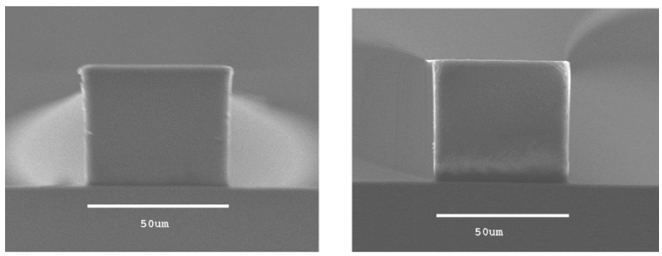

Fig. 4. Cross-sectional views of an SU-8 photoresist pattern for various exposure conditions (exposure: 300 mJ/cm^2) (a) with a UV-34 filter and (b) with a UV-34 filter and index-matching oil.

However, there is a limitation for choosing material due to the lack of materials that have optical transparency in the interested region and photosensitivity. Hot embossing and molding are indirect fabrication techniques by means of transferring the waveguide structure on the substrate. The embossing plate or cast is first fabricated using the master waveguide pattern. Once the plate or the cast was fabricated, the rest of processes are purely replication steps. Therefore, these fabrication techniques are suitable for mass production, such as the stamping of a compact disk. Laser ablation technique is similar to carving without using a chisel. A highly intensive UV laser beam removes the material of unwanted region. The motion stage, which holds the waveguide substrate, is moved along the predefined paths. Therefore, processing time is quite long. It is a very versatile tool for small quantities in fabrication and does not require a mask pattern.

The molding method was chosen in this experiment because of its dependable process and suitability for large-volume production, even though only a small quantity is needed in the research stage. Solid mold is generally used in various applications such as embossing, optical disk stamping, and Fresnel lens fabrication. The solid mold is made of nickel alloy by electroplating. The fabrication of the solid mold has higher cost and takes a long time. These reasons make us seek alternative mold materials. Curable resins such as silicone and urethane can be used as an alternative to reduce the fabrication

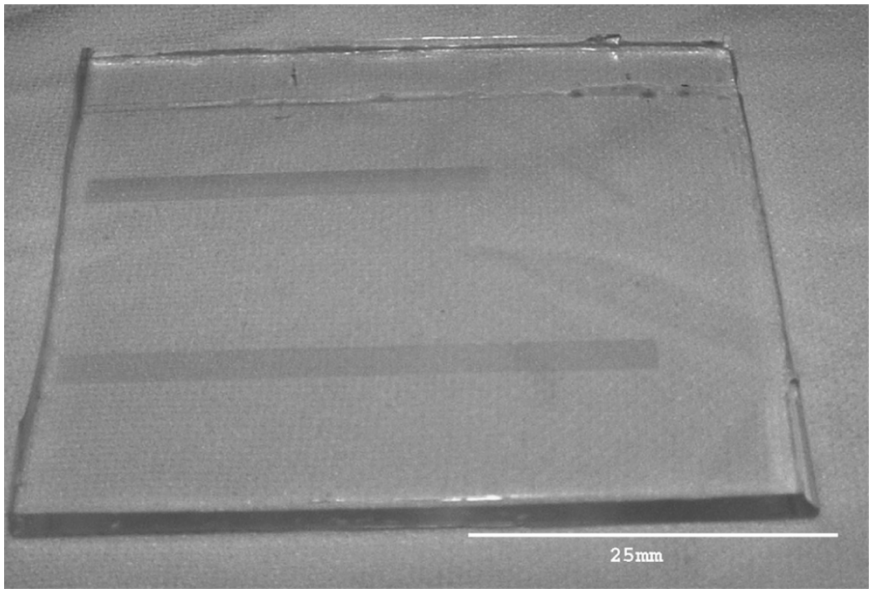

Fig. 5. PDMS waveguide mold.

cost and time. The soft mold has been used in various applications such as rubber stamp, small-quantity manufacturing, replication, and micromachining.

The mold is a negative copy of the master structure. Once the master is fabricated, making the mold is simply pouring a mold material over the master and curing. A silicone elastomer, especially poly(dimethylsiloxane) (PDMS) was chosen to fabricate the mold. The master for the mold was fabricated on an Si-wafer. The multimode waveguide is required for board-level interconnection because of the requirement of the lower packaging cost. Alignment of the devices (laser and detector) and the waveguide is easer when the core size of the waveguide is large. The designed size of the multimode waveguide is 50×50 μm. The process is the same as standard photolithography. The Piranha bath consists of two parts of sulfuric acid (H_2SO_4) and one part of hydrogen peroxide (H_2O_2). An Si-wafer was cleaned in the Piranha bath. After the cleaning, the wafer was baked at 150 °C to remove adsorbed water just before spin coating. This baking step improves adhesion and removes bubbles in the prebaking step. After baking, photoresist (SU8-2000 by MicroChem) was poured on the wafer and then spin-coated at 400 r/min for 5 s and then ramped to 1500 r/min for 40 s. The wafer stayed on a leveled surface for 5 min to improve uniformity. And then, the wafer was moved to a leveled hot plate for a prebake. The prebake was carried out at 65 °C for 5 min and 90 °C for 40 min. The photoresist tends to have negative sloped side wall, which is not good for mold application. The side wall should have positive slope or at least be vertical for mold application. An exaggerated negative wall is often called a T-topping. The T-topping results from the lateral diffusion of the acid near the surface. UV lights shorter than 350 nm are absorbed strongly at the top surface of the photoresist; hence, acid is generated by UV, which diffuses laterally on the top surface. The T-topping can be removed by filtering out short wavelengths below 350 nm [26]. A nearly vertical side wall [Fig. 4(a)] was made using short-wavelength cut filter (UV-34 by Hoya). However, there is still a beak-shaped feature between the side walls and top surface. The beak shape results from the diffraction at the interface between the mask and the photoresist, and it can be eliminated by filling index-matching oil (glycerol) into the gap [27]. Ethylene glycol, instead of glycerol, was used to fill the air gap in this experiment. The beak was completely removed [Fig. 4(b)].

The mold material is PDMS (Sylgard 184 by Dow Corning). A prepolymer and curing agent were mixed at a 1:10 ratio. Air bubbles trapped in the PDMS were removed in a vacuum chamber. After removing the air bubbles, the PDMS was poured on the master and cured at 90 °C in a vacuum chamber for 10 h. Surface relief structures were transferred from the master to the mold. The PDMS mold is shown in Fig. 5.

V. Flexible Optical Waveguide Film Fabrication

The fully embedded board-level optical interconnection requires a thin, flexible optical layer. Current electroplating technology can easily plate a through-hole or a via having an aspect ratio of 1 in the production line and can plate a hole having an aspect ratio of 3 in the laboratory. The size of a typical electrical pad on the device is about 100 μm. These are main reasons for the thickness limit of the substrate film. The thin and flexible optical waveguide layer was fabricated by a compression-molding technique using soft mold. A 127-μm-thick optically transparent film (Topas 5013) was used as a substrate of the waveguide circuit.

The fabrication step is straightforward. First, core material (SU-8) was poured on the heated PDMS, which is kept at 50 °C [Fig. 6(a)]). The heated PDMS mold suppresses bubble generation during the molding process. Then, excess SU-8 was scraped out using a squeegee [Fig. 6(b)]. The squeegee was made of PDMS, as well. The Topas film was applied on the top of the PDMS mold filled with SU-8. In the next step, the mold and the Topas film were inserted into the press machine, and then the pressure was applied for 30 min while the plunge plate

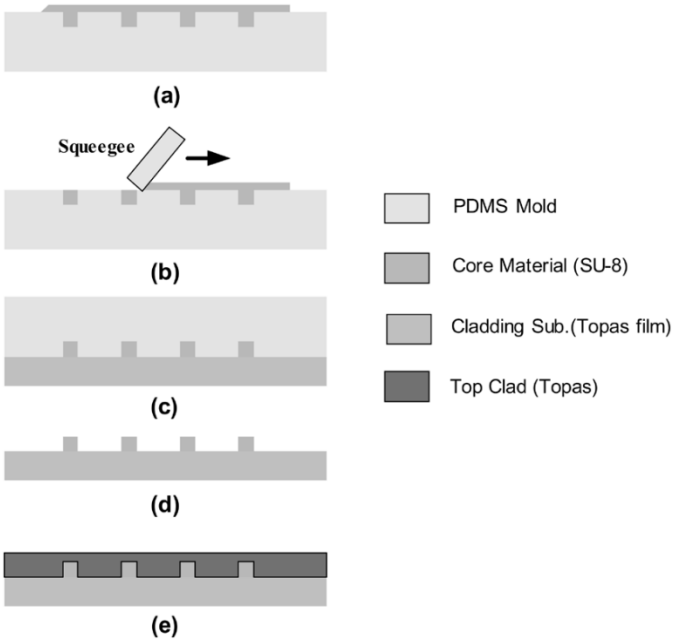

Fig. 6. Flexible optical waveguide film fabrication process flow. (a) Core material (SU-8) applied. (b) Excess material removed. (c) Heat and pressure applied on the mold and cladding substrate. (d) Plunger cooled down and released. (e) Top-cladding materials applied (either spin coat or lamination).

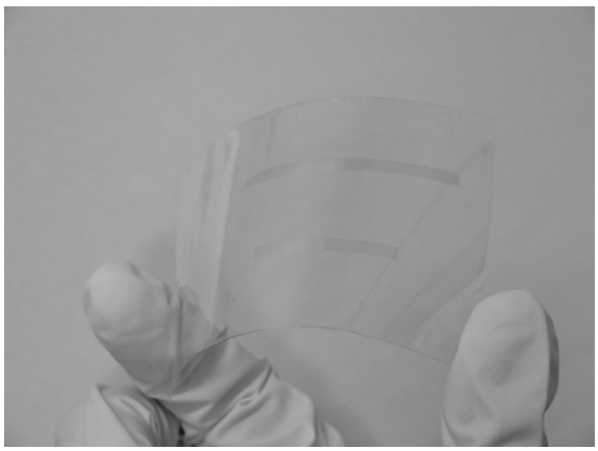

Fig. 7. Fabricated flexible optical waveguide film.

was held at 90 °C [Fig. 6(c)]. The cooling-down procedure was followed. In this procedure, the mold pressure decreased gradually due to the thermal contraction. The core material (SU-8) was transferred to the substrate film [Fig. 6(d)]. In the next step, the substrate film without the top cladding was exposed to UV to cross-link the SU-8. Once the film is exposed, it becomes chemically and thermally stable. Aluminum was deposited on the mirror facets in a vacuum chamber to make the mirror. Finally, the top cladding material (Topas) was coated on the film. The fabricated optical interconnection layer is shown in the Fig. 7. It has micromirror couplers and 12 channel waveguides of 50 mm in length. The measured absorption losses of the Topas material (substrate film) are 0.01 dB/cm and 0.03 dB/cm at 630 nm and 850 nm, respectively (Fig. 8). P. D. Curtis reported 6-dB/cm propagation loss at 850 nm for a multimode SU-8 waveguide [28]. W. H. Wong *et al.* eported

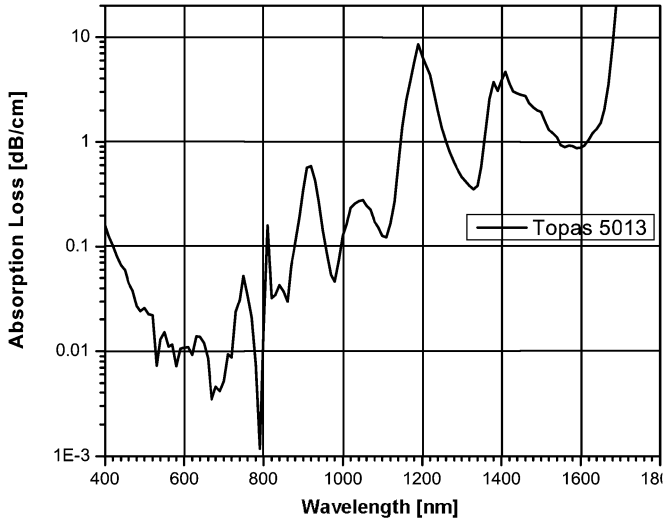

Fig. 8. Extracted absorption loss of the Topas 5013 as a function of wavelength.

a low propagation loss of 0.22 dB/cm and 0.48 dB/cm at 1330 nm and 1550 nm, respectively, using electron-beam direct writing [29]. Waveguide propagation loss was measured by the cutback method. The core dimension was 50×50 μm. The fiber pigtailed 850-nm laser was used to couple the laser to waveguide. The diameter of fiber is 10 μm, which is similar to the VCSEL aperture. Coupled-out powers are shown in Fig. 9, according to the length. The measured propagation loss was 0.6 dB/cm at the 850-nm wavelength. The lights coupled out from 45° mirrors are shown in Fig. 10. An He–Ne laser is launched at the ends of the waveguides. Lights came out at 45° mirrors, which are located at the other ends of waveguides.

VI. Thermal Management of the Buried VCSEL

The VCSEL is a major heat source in fully embedded guided-wave optical interconnects. The embedded VCSEL arrays are thermally isolated by surrounding insulators; therefore, heat builds up, and the operating temperature increases. The thermal management of the VCSEL is important because of reliability concerns. The embedded VCSEL cannot be replaced to repair in a fully embedded integration; therefore, we have to be aware of a good VCSEL before the integration and provide an optimal operating condition. Effective heat removal is a challenging task in the embedded structure because we have to consider packaging compatibility to the PCB manufacturing process while providing an effective and simple cooling mechanism.

The innovated heat management system for the fully embedded approach is introduced. The key idea is using an n-contact metal affiliated with the bottom distributed Bragg reflector (DBR) mirror of the VCSEL die as a heat spreader and a part of the heat sink by directly electroplating with copper during the integration process. Usually, copper that is several tens of micrometers thick was deposited in a copper-contained acid chemical solution during the PCB process. The direct bonding of the device using Cu electroplating reduces thermal resistance of the device due to the absence of the lower thermal conductivity bonding epoxy.

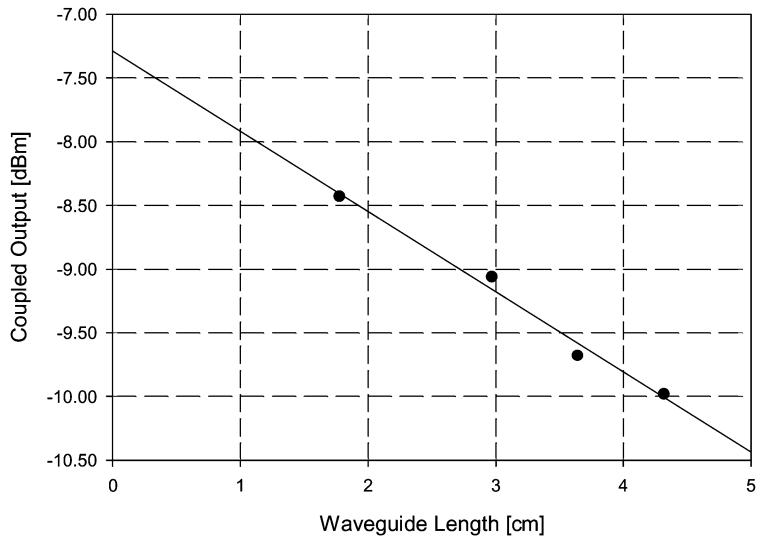

Fig. 9. Coupled-out power as a function of waveguide length. (Cutback method: the slope of the line is propagation loss, and the propagation loss is 0.6 dB/cm at an 850-nm wavelength).

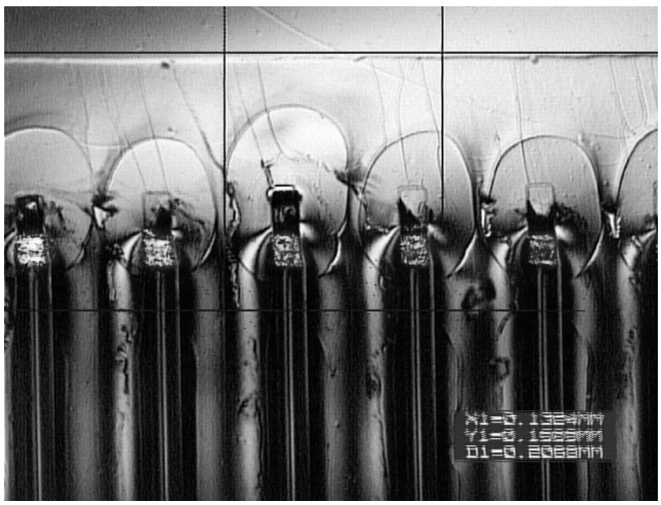

Fig. 10. Coupled-out beams from 45° waveguide mirrors. (Flexible waveguide: the 633-nm He–Ne laser was launched from the other side of the waveguide).

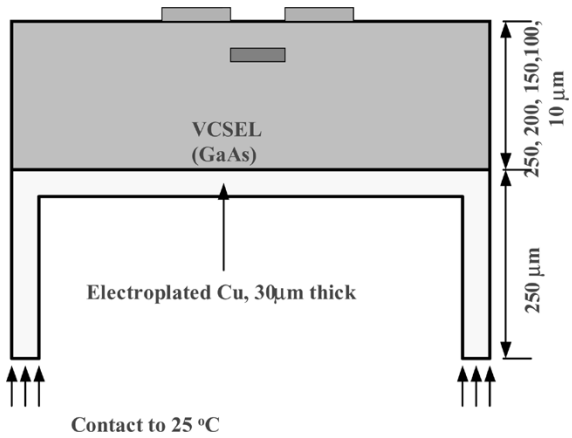

Fig. 11. Embedded heat-sink structure (VCSELs of various thicknesses with 30-μm-thick electroplated copper film).

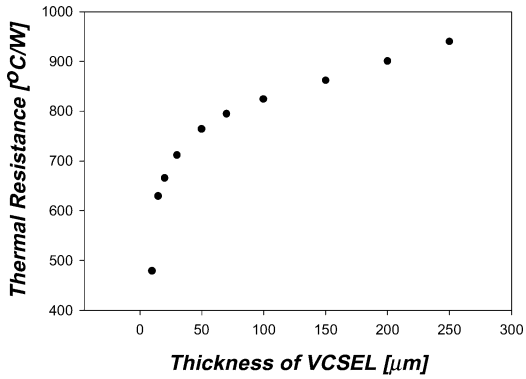

Fig. 12. Thermal resistances of VCSELs of various thicknesses with 30-mm-thick directly electroplated copper heat sink. (Active area : Diameter of 18 μm. Power dissipation: 20 mW).

ANSYS software was used to perform a two-dimensional (2-D) finite-element thermal distribution analysis. The heat transfer model configuration for the embedded heat-sink structure is shown in Fig. 11. The thermal conductivities of GaAs, the DBR mirror, and copper are 4.6×10^{-5} W/μm $\cdot$ K, 2.3×10^{-5} W/μm $\cdot$ K, and 4×10^{-4} W/μm $\cdot$ K, respectively. As VCSEL parameters, an active diameter of 18 μm, a thickness of 0.3 μm, and a power dissipation of 20 mW were used [30].

Theoretically determined thermal resistances for VCSELs with various thicknesses are shown in Fig. 12. For a 30-μm-thick electroplated copper film, the junction temperatures were theoretically determined to be 43.8, 43, 42.2, 41.5, 40.2, and 34.6 °C for 250, 200, 150, 100, 50, and 10-μm-thick VCSELs, respectively. The substrate-removed VCSEL having a total thickness of 10 μm shows superior optical and thermal characteristics.

Although the substrate-removed VCSEL has superior properties, fabrication and handling are very difficult. If we assume that the thermal resistance of the normal-thickness VCSEL (250 μm thick) packaged on a bulk copper heat sink is a reference (722 K/W) for reliable operation, the maximum thickness

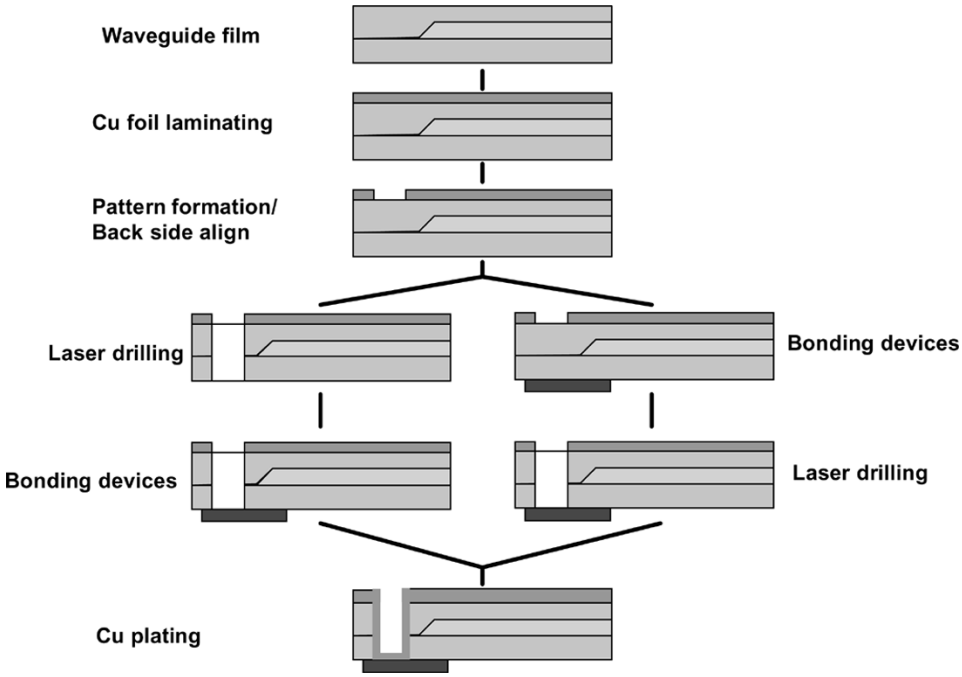

Fig. 13. Device integration process flowchart.

of an embedded VCSEL will be 50 μm according to simulation results. A device several tens of micrometers thick can be easily fabricated, and handling of the device is much easier.

VII. Device Integration on Flexible Waveguide Film

The integration of optoelectronic devices with the flexible waveguide film is the most important process among the whole integration steps, including the final laminating process with the PCB. The flexible waveguide film has the thickness of 127 μm. The VCSEL and photodetector arrays have a diameter of about 95 μm. In general, copper electroplating allows plating of a via with an aspect ratio of 1; however, it is possible to plate a via with an aspect of 3 in a laboratory environment. The maximum diameter of the laser drilled via is limited by the pad size of devices, the aspect ratio, and the registration error during the lamination process. Fig. 13 illustrates the device integration process. First, copper foil 1 mil (25.4 μm) thick is laminated on the top of the flexible waveguide layer by applying heat and pressure. Then, this copper foil is patterned to form the top electrical pads for the VCSEL and photodetector. The main reason for the formation of the laminated copper foil is the limitation of electroplating. The thickness of additional electrical layers easily exceeds 1 mm, and the diameter of the device pad is 95 μm. This translates to an aspect ratio of 100; therefore, this hole cannot be electroplated. The aspect ratio of the via can be reduced by introducing the copper foil just above the waveguide layer; hence, we can electroplate microvia. Furthermore, the patterns on the copper foils can be bigger. This means that a larger registration error can be allowed during the laminating process with electrical layers.

The next step is either laser drilling or device bonding on the waveguide layer. There is a possibility of damaging device pads during laser microvia drilling. If damage happens, the device-bonding step follows drilling. The bonding of devices was performed using an aligner. The typical aligner has two holders: one for the mask, and the other for the substrate. The flexible waveguide film was temporally bonded to a clear glass plate using water and placed on a mask holder. The device to be integrated was put on the substrate holder. A small amount of UV-curable adhesive was applied on the top of the device. When the device and waveguide micromirror coupler were aligned, they were exposed with UV to cure the adhesive.

The bonding of the device to the waveguide film can be accomplished by melt-bonding without using a UV-curable adhesive. When alignment is completed, the device is heated just above the melting temperature of the waveguide film for a short period. In addition, the device is bonded to the waveguide film without deforming the microvias. The flexible optical interconnection layer with device integration is shown in Fig. 14. There is no microvia. The length of the waveguide is 50 mm. 1×12 VCSEL and p-i-n photodetector arrays were bonded at a precise location. Micromirror couples are clearly shown in the enlarged picture.

VIII. Conclusion

Thermal runaway of the embedded VCSEL is the critical concern due to the reliable operation of VCSELs for a long time. This paper described the investigation of an effective heat-sink structure for VCSELs through the 2-D finite-element thermal analysis. The 30-μm-thick directly electroplated copper film on the back side of VCSEL array turns out to be an excellent heat sink without sacrificing the strategy of easy packaging. The maximum thickness of VCSELs, which guaranteed reliable operation, were also found. Extremely thin VCSELs are very difficult to handle. As it turns out, 50 μm is the maximum thickness for a reliable operation in a fully embedded structure. This thick device can be handled by a state-of-the-art automated pick-and-place machine.

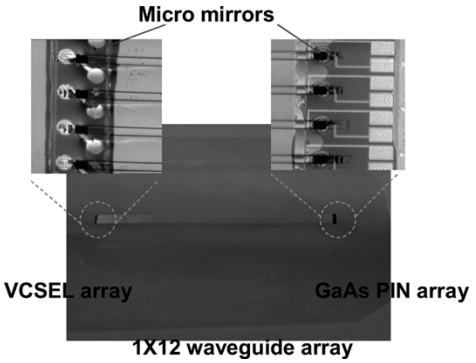

Fig. 14. Integrated VCSEL and detector arrays on a flexible optical waveguide film.

45° waveguide micromirror couplers were fabricated by cutting waveguide ends at 45° using a microtome blade. The coupling efficiency of an aluminum-coated micromirror was calculated. The coupling efficiency between the 12-μm-aperture VCSEL mounted at the bottom of a 127-μm-thick cladding layer and a 50 $\times$ 50-μm waveguide was 92%, ignoring the reflectance of aluminum by nearly 100%. The coupling efficiency did not change within a $\pm 1.5°$ angular deviation from 45°. The optical interconnection layer was fabricated by a compressive soft-molding process. The micromirrors and waveguides were fabricated on the flexible substrate film at the same time. The core material of the waveguide was SU-8. The measured propagation loss of the waveguide was 0.6 dB/cm at 850 nm.

REFERENCES

[1] D. P. Seraphim and D. E. Barr, "Interconnect and packaging technology in the 90's," in *Proc. SPIE.*, vol. 1390, 1990, pp. 39–39.
[2] R. O. C. Neugerbauer, R. A. Fillion, and T. R. Haller, "Multichip module designs for high performance applications," in *Multichip Modules, Compendium of 1989 Papers: International Electronic Packaging Society*, vol. 149, 1989.
[3] International SEMATECH, "The National Technology Roadmap for Semiconductors (ITRS)—Technology Needs," Semiconductor Industry Association, 2000.
[4] N. Cravotta, "Wrestlemania: Keeping high-speed-backplane design under control," *EDN*, pp. 36–46, Aug. 22, 2002.
[5] L. W. Schaper, "Flex and the interconnected mesh power system," in *Foldable Flex and Thinned Silicon Multichip Packaging Technology*. Norwood, MA: Kluwer, 2003, ch. 12.
[6] R. C. Walker, K. C. Hsieh, T. A. Knotts, and C. S. Yen, "A 10 Gb/s Si-bipolar TX/RX chipset for computer data transmission," in *Proc. IEEE Int. Solid-State Circuits Conf.*, vol. 302, Feb. 1998, pp. 302–303.
[7] M. Gruber, S. Sinzinger, and J. Jahns, "Optoelectronic multichip module based on planar-integrated free-space optics," in *Proc. SPIE, Optics Computing 2000*, vol. 4089, 2000.
[8] G. Kim and R. T. Chen, "Three-dimensionally interconnected multi-bus-line bidirectional optical backplane," *Opt. Eng.*, vol. 38, pp. 9–9, 1999.
[9] E. Griese, "Parallel optical interconnects for high performance printed circuit board," in *Proc. 6th Int. Conf. Parallel Interconnects (PI'99)*, Oct. 1999, pp. 173–173.
[10] Y. Ishii, S. Koike, Y. Aria, and Y. Ando, "SMT-compatible optical I/O chip packaging for chip-level optical interconnects," in *Proc. Electronic Components Technology Conf. (ECTC)*, 2001, pp. 870–875.
[11] D. Krabe, F. Ebling, N. Arndt-Staufenbiel, G. Lang, and W. Scheel, "New technology for electrical/optical systems on module and board level: The EOCB approach," in *Proc. 50th Electronic Components Technology Conf.*, May 2000, pp. 970–970.
[12] T. Suhara and H. Nishihara, "Integrated optics components and devices using periodic structures," *IEEE J. Quantum Electron.*, vol. QE-22, pp. 845–845, June 1996.
[13] D. Brundrett, E. Glystis, and T. Gaylord, "Homogeneous layer models for high-spatial-frequency dielectric surface-relief gratings," *Appl. Opt.*, vol. 33, pp. 2695–2695, 1994.
[14] D. Y. Kim, S. K. Tripathy, L. Li, and J. Kumar, "Laser-induced holographic surface relief gratings on nonlinear optical polymer films," *Appl. Phys. Lett.*, vol. 66, pp. 1166–1166, 1995.
[15] R. T. Chen, F. Li, M. Dubinovsky, and O. Ershov, "Si-based surface-relief polygonal gratings for 1-to-many wafer-scale optical clock signal distribution," *IEEE Photon. Technol. Lett.*, vol. 8, 1996.
[16] R. K. Kostuk, J. W. Goodman, and L. Hesselink, "Design considerations for holographic optical interconnects," *Appl. Opt.*, vol. 26, pp. 3947–3947, 1987.
[17] L. Eldada and J. T. Yardly, "Integration of polymeric micro-optical elements with planar waveguiding circuits," in *Proc. SPIE*, vol. 3289, 1998, pp. 122–122.
[18] R. T. Chen, L. Lin, C. Choi, Y. Liu, B. Bihari, L. Wu, R. Wickman, B. Picor, M. K. Hibbs-Brenner, J. Bristow, and Y. S. Liu, "Fully embedded board-level guided-wave optoelectronic interconnects," *Proc. IEEE*, vol. 88, pp. 780–793, June 2000.
[19] M. Kagami, A. Kawasaki, and H. Ito, "A polymer optical waveguide with out of plane branching mirrors for surface-normal optical interconnections," *J. Lightwave Technol.*, vol. 19, pp. 1949–1955, Dec. 2001.
[20] H. Terui, M. Shimokozono, M. Yanagisawa, T. Hashimoto, Y. Yamashida, and M. Horiguchi, "Hybrid integration of eight channel PD-array on silica based PLC using micro-mirror fabrication technique," *Electron. Lett.*, vol. 32, no. 18, 1996.
[21] Hikita, R. Yoshimura, M. Usui, S. Tomaru, and S. Imamura, "Polymeric optical waveguides for optical interconnections," *Thin Solid Films*, no. 331, pp. 303–303, 1998.
[22] K. D. Choquette and K. M. Geib, "Fabrication and performance of vertical cavity surface emitting lasers," in *Vertical Cavity Surface Emitting lasers*, C. Wilmsen, H. Temkin, and L. A. Coldren, Eds. Cambridge, U.K.: Cambridge Univ. Press, 1999, ch. 5 .
[23] H. J. Unold, S. W. Z. Mahmoud, R. Jager, M. Kicherer, M. C. Riedl, and K. J. Ebeling, "Improving single-mode VCSEL performance by introducing a long monolithic cavity," *IEEE Photon. Technol. Lett.*, vol. 12, pp. 939–939, Aug. 2000.
[24] N. Nishiyama, M. Arai, S. Shinada, K. Suzuki, F. Koyama, and K. Iga, "Multi-oxide layer structure for single-mode operation in vertical-cavity surface-emitting lasers," *IEEE Photon. Technol. Lett.*, vol. 12, pp. 606–606, June 2000.
[25] D.-S. Song, S.-H. Kim, H.-G. Park, C.-K. Kim, and Y. H. Lee, "Single-mode photonic-crystal vertical cavity surface emitting laser," in *Conf. Lasers Electro-Optics (CLEO '02) Tech. Dig.*, vol. 1, 2002, pp. 293–293.
[26] Micorchem Product References. Microchem, Newton, MA. [Online]. Available: http://www.microchem.com/products/pdf/SU8_2035-2000.pdf
[27] Y. J. Chuang, F. G. Tseng, and W. K. Lin, "Reduction of diffraction effect of UV exposure on SU-8 negative hick photoresist by air gap elimination," *Microsystems Technologies*, vol. 8, pp. 308–308, 2002.
[28] P. D. Curtis, S. Iezeliel, R. E. Miles, and C. R. Pescod, "Preliminary investigations into SU-8 as a material for integrated all-optical microwave filters," in *High Frequency Postgraduate Student Colloquium, 2000*, vol. 7–8, Sept. 2000, pp. 116–120.
[29] W. H. Wong, J. Zhou, and E. Y. B. Pun, "Low-loss polymeric optical waveguides using electron-beam direct writing," *Appl. Phys. Lett.*, vol. 78, pp. 2110–2110, 2001.
[30] C. Choi, L. Lin, Y. Liu, and R. T. Chen, "Performance analysis of 10 μm thick VCSEL array in fully embedded board level guided-wave optoelectronic interconnects," *J. Lightwave Technol.*, vol. 21, pp. 1531–1535, June 2003.

Chulchae Choi was born in Inchon, Korea, on May 1, 1966. He received the B.S. and M.S. degrees in physics from Inha University, Incheon, Korea, in 1989 and 1991, respectively, and the Ph.D. degree in electrical and computer engineering from the University of Texas at Austin in 2003.

Lei Lin (M'03) received the B.S. degree in material science from LanZhou University, Lanzhou, China, the M.S. degree in electrical engineering from the University of North Carolina, Charlotte, and the Ph.D. degree in electrical engineering in optoelectronic interconnects from the University of Texas at Austin in 2003.

His research interests are in optical interconnects, polymer-based waveguide devices, and semiconductor photonic devices.

Dr. Lin is a Member of the American Physical Society (APS).

Yujie Liu received the B.S. and M.S. degrees in electronic science from Nankai University, Tianjin, China, in 1995 and 1998, respectively, and the Ph.D. degree in electrical engineering from the University of Texas at Austin in 2004.

Her area of research is in optical interconnects, optoelectronic devices, and optoelectronic integration.

Jinho Choi received the B.S. and M.S. degrees in materials science and engineering from Hong-Ik University, Seoul, Korea, in 1992 and 1994, respectively. He is currently working toward the Ph.D. degree in M.S.E. at the University of Texas at Austin.

In 1994, he joined Hyundai Central Research Institute, Suwon, Korea. His current research area is optoelectronic devices and chip-to-chip optical interconnection.

Li Wang received the B.E. degree in thermal engineering from the University of Science and Technology, Beijing, China, in 1992 and the M.S. degree in thermal engineering from the Institute of Engineering Thermophysics, Chinese Academy of Sciences, Beijing, China, in 2001. She is currently working toward the Ph.D. degree with the Department of Electrical and Computer Engineering at the University of Texas at Austin.

She worked as an Engineer in Beijing Central Engineering and Research Incorporation of the Iron and Steel Industry, China, from 1992 to 1998. Her current research area is board-level guided-wave optical interconnects.

David Haas, photograph and biography not available at the time of publication.

Jerry Magera, photograph and biography not available at the time of publication.

Ray T. Chen (M'91–SM'98–F'03) received the B.S. degree in physics from National Tsing-Hua University, Hsinchu, Taiwan, R.O.C., in 1980 and the M.S. degree in physics and the Ph.D. degree in electrical engineering, both from the University of California, San Diego and Irvine, in 1983 and 1988, respectively.

He worked as a Research Scientist, Manager, and Director of the Department of Electrooptic Engineering in the Physical Optics Corporation, Torrance, CA, from 1988 to 1992. He joined the University of Texas at Austin (UT Austin) as a faculty member to start the optical interconnect research program in the Electrical and Computer Engineering Department in 1992, where he has been the Temple Foundation Endowed Professor since 1998. He also served as the Chief Technology Officer/Founder and Chairman of the Board of Radiant Photonics from 2000 to 2001, where he raised $18 million dollars in A-Round funding to commercialize polymer-based photonic devices. His research group has been awarded with more than 60 research grants and contracts from such sponsors as the Department of Defense (DOD), the National Science Foundation (NSF), the Department of Energy (DOE), the National Aeronautics and Space Administration (NASA), the State of Texas, and private industry. He has served as a consultant for various federal agencies and private companies. His research topics have focused on two main subjects: polymer-based guided-wave optical interconnection and packaging and true-time-delay (TTD) wide-band phased-array antennas (PAAs). Experiences garnered through these programs in polymeric material processing and device integration are pivotal elements for the research work reported herein. His group at UT Austin has reported its research findings in more than 350 published papers, including more than 40 invited papers. He holds 12 issued patents.

Dr. Chen is a Fellow of the Optical Society of America (OSA) and the International Society of Optical Engineering (SPIE). He has chaired or has been a program committee member for more than 50 domestic and international conferences organized by the IEEE, the SPIE, the OSA, and Photonics Society of Chinese Americans (PSC), and he has delivered numerous invited talks to professional societies. In National Tsing-Hua University, he received the national championship of the national debate contest in Taiwan in 1979. He also received the 1987 University of California Regent's dissertation fellowship and the 2000 University of Texas Engineering Foundation Faculty Award for his contributions in research, teaching, and services.